ACS NANO
Cite This: ACS Nano 2019, 13, 12851−12859
www.acsnano.org

ARTICLE

Strong Electroosmotic Coupling Dominates Ion Conductance of 1.5 nm Diameter Carbon Nanotube Porins

Yun-Chiao Yao,[†,‡] Amir Taqieddin,[§] Mohammad A. Alibakhshi,[∥] Meni Wanunu,[∥] Narayana R. Aluru,[§] and Aleksandr Noy*[,†,‡]

[†]Physics and Life Sciences Directorate, Lawrence Livermore National Laboratory, Livermore, California 94550, United States
[‡]School of Natural Sciences, University of California Merced, Merced, California 95344, United States
[§]Department of Mechanical Science and Engineering, Beckman Institute for Advanced Science and Technology, University of Illinois at Urbana−Champaign, Champaign, Illinois 61820, United States
[∥]Department of Physics, Northeastern University, Boston, Massachusetts 02120, United States

Supporting Information

ABSTRACT: **Extreme confinement in nanometer-sized channels can alter fluid and ion transport in significant ways, leading to significant water flow enhancement and unusual ion correlation effects. These effects are especially pronounced in carbon nanotube porins (CNTPs) that combine strong confinement in the inner lumen of carbon nanotubes with the high slip flow enhancement due to smooth hydrophobic pore walls. We have studied ion transport and ion selectivity in 1.5 nm diameter CNTPs embedded in lipid membranes using a single nanopore measurement setup. Our data show that CNTPs are weakly cation selective at pH 7.5 and become nonselective at pH 3.0. Ion conductance of CNTPs exhibits an unusual 2/3 power law scaling with the ion concentration at both neutral and acidic pH values. Coupled Navier−Stokes and Poisson−Nernst−Planck simulations and atomistic molecular dynamics simulations reveal that this scaling originates from strong coupling between water and ion transport in these channels. These effects could result in development of a next generation of biomimetic membranes and carbon nanotube-based electroosmotic pumps.**

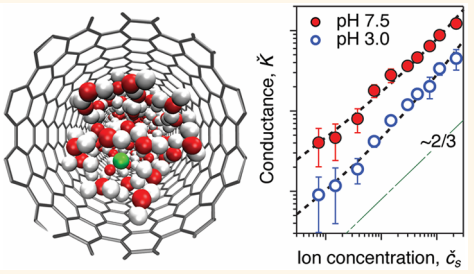

KEYWORDS: *nanofluidics, carbon nanotube porins, ion transport, slip-flow coupling, electroosmosis*

Ion transport and associated ionic equilibria feature prominently in a variety of condensed phase phenomena from energy storage in batteries[1] and colloidal stability[2] in materials science to plant growth[3] and nerve signal propagation in biology.[4] A large number of these phenomena involves ions traveling through and interacting in confined spaces that typically reach nanoscale dimensions. Extensive studies of colloidal and electrokinetic phenomena have revealed a detailed picture of ion interactions at distances from hundreds to tens of nanometers,[5,6] and the development of microfluidics has taught us much about the dynamics of fluid and ion transport in channels in this size regime.[6] At the same time, biophysicists who studied transport in biological ion channels were revealing efficient transport mechanism and unusual selectivity patterns of subnanometer diameter nanopores where water is squeezed down to molecular dimensions and often adopts a single-file configuration that is drastically different from that of the bulk state.[7] A number of those effects and mechanisms were reproduced and validated in synthetic model nanofluidic channels.[8,9] Yet we still lack detailed knowledge of water and ion behavior in the channels that fall into the intermediate regime of 1−10 nm pore size. These "single digit nanopores" are small enough to severely confine the ions and fluid, yet still too large to force the dramatic hydrogen-bond rearrangement of water molecules and partial loss of ion hydration shells that characterizes transport in single-file channels.[6] The existing studies of transport in these channels have already revealed a wealth of interesting physical phenomena including enhanced water transport in carbon nanotubes (CNTs),[9−11] strong electroosmotic coupling in boron nitride nanotubes,[12] and unusual modes of water transport in graphene and graphene oxide-based membranes.[13,14] Ion transport studies also revealed scaling relationships[15] that deviated from the concentration scaling expected for microchannels.[16,17] To study the details of these phenomena, we need model systems that offer reproducible and consistent channel features covering this size regime.

Received: June 29, 2019
Accepted: November 4, 2019
Published: November 4, 2019

DOI: 10.1021/acsnano.9b05118
ACS Nano 2019, 13, 12851−12859

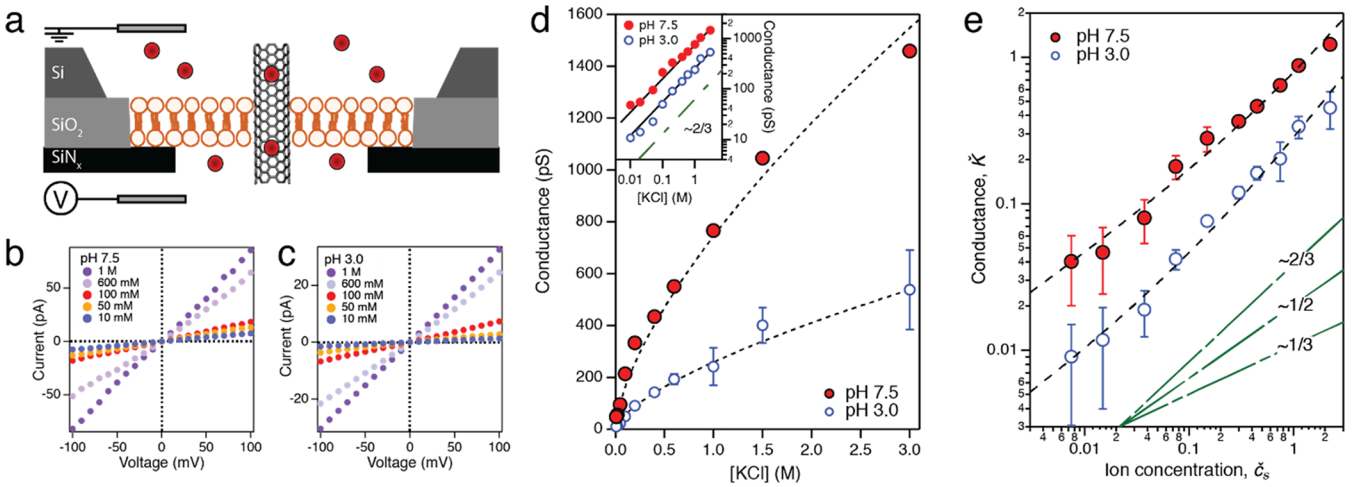

Figure 1. Ionic conductance of 1.5 nm diameter wCNTPs. (a) Schematics of the experimental setup where a small area lipid bilayer with a single CNTP is formed over a SiN_x nanopore. (b, c) *I*–*V* curves recorded for individual CNTPs at different KCl concentrations at pH 7.5 (b) and at pH 3.0 (c). (d) Individual CNTP ionic conductance as a function of KCl concentration at pH 7.5 and pH 3.0. Inset shows the data plotted on a log–log scale. Lines on both graphs are best fits of the data to a power law. (e) Conductance *vs* KCl concentration data from (d) replotted in dimensionless coordinates defined by eqs 2 and 3. Dashed lines are best fits to eq 1. Green dash-dotted lines correspond to different power law scaling and are presented only as a guide to the eye.

CNTs are good candidates for such model channels because of their relatively simple structure—smooth hydrophobic inner channel surface and the localized controllable charges at the pore entrances[18]—and well-defined diameters that fall squarely into the "single digit nanopore" range. Simulations and experimental studies of water and ion transport in CNT pores showed fast high-slip water flow,[8,9,11,19] unusual ion selectivity, and conductance scaling,[9,15] and electrophoretically induced water flows.[20]

We have recently reported carbon nanotube porins (CNTPs),[9,21,22] ultrashort CNT fragments that can self-insert into the lipid bilayers and form biomimetic membrane pores. Our previous studies showed that 0.8 nm diameter CNTPs (nCNTPs), which force water into a single-file configuration,[9] show highly nonlinear conductance *vs* ion concentration characteristics attributed to the ion interactions with the negatively charged carboxyl groups at the CNTP entrance. This negative charge was also responsible for the very high cation selectivity of these channels, and at low ion concentrations, the pore conductance followed the $c^{1/2}$ concentration scaling characteristic for the good co-ion exclusion conditions.[9,23] In this work, we report the ion conductance characteristics and selectivity of the wider 1.5 nm diameter CNTPs (wCNTPs), compare measured ion transport behavior with that of the narrower nCNTPs, and study the effects of the charge on the CNTP entrance on the ion conductance. We also perform continuum simulations using Navier–Stokes and Poisson–Nernst–Planck (NS-PNP) model and molecular dynamics (MD) simulations to show that the dominant contribution to the power law scaling of the concentration-ionic conductance relation comes from the electroosmotic coupling effects. The overall physical picture that emerges shows tightly coupled water and ion flows in these nanopores.

RESULTS AND DISCUSSION

CNTP Conductance Measurements. We synthesized wCNTPs using sonication-assisted cutting of μm-long CNT feedstocks in the presence of lipid molecules, which stabilized cut CNTs in water. For measuring ion conductance of individual CNTPs, we used a modified planar lipid bilayer setup (Figure 1a) that we developed for our previous studies. This setup was based on a small *ca.* 100 nm diameter nanopore etched in a thin SiN_x film supported over a larger opening on a silicon wafer.[9] SiN_x film provides a clean hydrophilic surface onto which we fused lipid vesicles containing CNTPs. This platform offers several significant advantages over traditional planar lipid membrane platforms, including the ability to control the number of CNTPs in the bilayer, reduction in the bilayer undulations and the associated noise, and the ability to use completely solvent-free bilayers. Current–voltage (*I*–*V*) curves recorded for wCNTPs in this setup (Figure 1b,c) were symmetric and showed linear dependence on applied voltage over two decades of KCl electrolyte concentrations, indicating that the dominant charge carrier ion species did not encounter a significant energy barrier when entering the nanotube pore.[24] wCNTP conductance at 1 M KCl concentration, measured from the slope of the *I*–*V* curve, 766 ± 49 pS, was close to the value of 630 ± 120 pS which we measured previously from the current jumps corresponding to the spontaneous wCNTP incorporation into lipid bilayer in a traditional planar lipid bilayer setup.[21] We attribute the slightly higher conductance value obtained in our current experiments to the use of solvent-free bilayers.

Conductance Scaling. wCNTP conductance exhibited a pronounced nonlinear dependence as a function of the KCl electrolyte concentration (Figure 1d). For most of the ion concentration range, conductance values followed a power law dependence with the exponent very close to the value of 2/3. This apparent 2/3 power law scaling is qualitatively different from the linear conductance dependence expected for ideal channels; it does not show the limiting surface conductance behavior of typical nanochannels with charged surfaces;[25] and it is also distinct from the conductance scaling reported previously for CNT channels.[15,17] It is reasonable that wCNTPs would not show the conductance saturation behavior of nCNTPs at high salt concentrations, which arises from a combination of single-file geometry of that channels and

DOI: 10.1021/acsnano.9b05118
ACS Nano 2019, 13, 12851–12859

charged groups at the nanotube entrance. Our data also do not follow the $c^{1/2}$ scaling reported by Nuckolls and colleagues for longer CNT channels with the similar 1.5 nm diameter[17] or the $c^{1/3}$ scaling measured by Bocquet and colleagues in larger 7−70 nm diameter CNTs.[15]

To elucidate the influence of the negative charges that usually decorate nanotube entrance on the ion transport through wCNTPs, we measured their conductance characteristics at pH 3.0 where the carboxylate ($-COO^-$) groups at the CNTP rim protonate and become neutral (−COOH). $I-V$ curves measured at pH 3.0 conditions (Figure 1c) also showed linear behavior at all tested values of electrolyte concentrations, indicating that the entrance charges do not contribute significantly to the pore entrance barriers. Notably, overall conductance at pH 3.0 is reduced relative to the values measured at pH 7.5, which is qualitatively consistent with the trends observed in experiments and in models.[15,23] This observation also rules out the possibility of protonic currents dominating CNTP conductance, unlike the behavior reported previously for ultralong CNT channels of similar diameter.[26]

The exact physical model describing ion conductance scaling in CNT pores has been the subject of intense scrutiny in recent research literature. Bocquet and co-workers postulated that inner surfaces of nanotube pores bear some negative charge due to adsorption of hydroxyl ions[27] and showed that charge regulation, combined with the PNP model for conductance, leads to the $c^{1/3}$ scaling of the ion conductance, a prediction that they confirmed experimentally by measuring ion conductance of large diameter (7−70 nm) CNTs.[15] Bieshuevel and Bazant described similar physics using a combined space-charge theory with the Donnan approximation and obtained an analytical expression for CNT conductance that predicted a limiting conductance scaling of $c^{1/2}$ at low ion concentrations,[23] the scaling that seems to be corroborated by the data of Nuckolls and co-workers on conductance of 1.5 nm diameter nanotubes incorporated into microfluidic measurement platform.[17] Recently Bonthuis and co-workers presented an detailed theoretical study that showed that conductance in nanotubes can exhibit several regimes characterized by power law exponents of 1, 1/3, or 1/2 and quantified the crossover between those regimes.[28]

Curiously, these models did not consider the nature of transport through CNTs that is characterized by very large wall slip and correspondingly very high rates of water transport.[9−11] One of the most interesting possibilities for ion transport in these pores is that large slip could lead to unusually high electro-osmotic and diffusion-osmotic coupling,[29,30] which should be significantly enhanced for small diameter CNT pores that exhibit very high slip. Even though a number of previous theoretical works mentioned this possibility in passing or alluded to it,[23] most have neglected the contribution of the electroosmotic term to the overall conductance. A rigorous analysis of this case was done only recently by Manghi and colleagues, who solved the Poisson−Boltzmann equation for cylindrical pores in the presence of charge regulation and high flow slip and identified several scaling regimes for conductivity.[30]

The most relevant of those regimes for our experiments is the low surface charge density regime, where the conductance arises from the combined contributions of a term representing ion migration and a term representing slip-enhanced electro-osmotic flow. Total conductance is then described as

$$\check{K} = 2\check{\mu}\left(\frac{\sigma^*}{2h}\check{c}_s\right)^{1/2} + (1 + 4\check{b})\frac{\sigma^*}{2h}\check{c}_s \tag{1}$$

where $\check{K}$ and $\check{c}_s$ are the dimensionless conductance and salt concentration, respectively, obtained from ion conductance, G, and electrolyte concentration, c_s as

$$\check{K} = G \times \frac{2\pi L \times {l_b}^2 \times \eta}{e^2} \tag{2}$$

$$\check{c}_s = \pi \times l_b \times r^2 \times c_s \tag{3}$$

where L and r are the pore length and radius, l_b is the Bjerrum length, η is the dynamic viscosity of the water, and h is a pH-dependent factor. The additional dimensionless parameters are σ^* the maximum surface charge density, $\check{\mu}$ is the ion mobility, and $\check{b}$ is the slip length (an empirical parameter defining the relative retardation of fluid velocity next to the fluid-wall interface) obtained from the corresponding dimensional parameters as

$$\sigma^* = \frac{\pi R l_b}{e}\sigma; \quad \check{\mu} = 2\pi\eta l_b \mu; \quad \check{b} = \frac{b}{r} \tag{4}$$

Eq 1 fits our wCNTP conductance data very well over the whole range of concentrations (Figure 1e) at both pH values that we investigated, reproducing the approximately 2/3 power law scaling observed in the experiment. However, the fits also indicate that the fitted values of slip length, b, differ significantly at different pH, changing from 1.1 nm at pH 7.5 to as much as 19.1 nm at pH 3.0 (see Table S1 in Supporting Information for the fitted values of the model parameters; note also that the fitted values of the surface charge parameter are consistent with the assumption of the low surface charge density regime). This observation points to an interesting possibility that the slip length in CNT pores may be a strong function of pH. This notion of pH-dependent slip length is also consistent with the physical picture of OH^- ion adsorption on the CNT walls, where those charges disrupt the slip flow conditions on the perfectly smooth CNT walls. Indeed, we would expect that OH^- adsorption to be diminished at low pH values and produce larger effective slip lengths, which is consistent with the results of the fit. Our previous experimental data also showed enhanced water flow in 1.5 nm diameter CNTPs at acidic pH values. We also note that although the values of the slip lengths obtained in our fits are significantly smaller than values reported in the literature,[10,11,19] this discrepancy likely reflects the difference between μm-long CNTs channels used in those studies and the ultrashort nanotubes used in the current work.

Coupled NS-PNP Continuum Simulations of Ion Transport. To investigate the contribution of electroosmotic coupling on the ionic conductance and to reduce reliance on the fitted parameters, we performed continuum simulations of the ion transport using the NS-PNP model and the concentration-surface charge dependence relation, $|\sigma| \sim c^{1/2}$ (see Supporting Information eqs S1−S14).[23] First, we computed the concentration-conductance scaling by solving only the PNP equations. Next, we solved the same system using the coupled NS-PNP equations to account for the contribution of the electroosmotic flow. Here, we simulated a CNT with d = 14 nm and L = 10 nm. The surface charge values are directly taken from the Biesheuvel and Bazant work for the same CNT size at pH = 6.[23] When the contribution

DOI: 10.1021/acsnano.9b05118
ACS Nano 2019, 13, 12851−12859

from the electroosmotic velocity is neglected, we observe a power law scaling with an exponent of *ca.* 0.49 (Figure 2a),

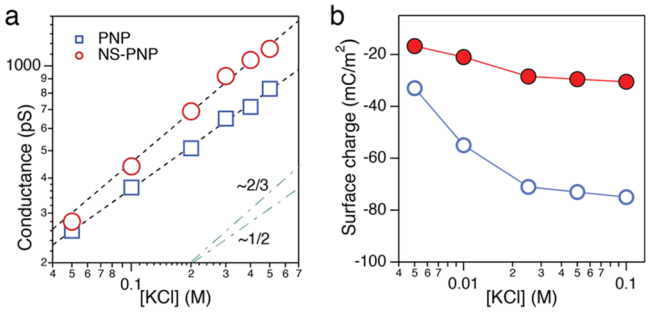

Figure 2. NS-PNP simulations of ion conductance in CNTPs. (a). Simulated conductance-concentration scaling in a CNTP using PNP model (blue squares) and combined NS-PNP model (red circles). Dashed lines correspond to power law ($G \sim c^{\alpha}$) fits to the data with the slopes of α = 0.49 for PNP and α = 0.62 for NS-PNP. (b) Calibrated effective surface charge of a CNTP of d = 1.5 nm and L = 10 nm based on the experimentally measured conductance at pH 3 (red circles) and at pH 7.5 (blue circles). Surface charge values were obtained from NS-PNP simulations and plotted as a function of ion concentration.

which followed the trend proposed by Biesheuvel and Bazant.[23] When the velocity effect is included, we observed that the conductance-concentration scaling exponent shifts to higher values and follows a higher exponent of *ca.* 0.62, indicating that indeed, as we observed in the experiments and as Manghi and co-workers predicted by analytical modeling, the ionic conductance is enhanced due to electroosmotic effects.[30]

Next, we calibrated the surface charge on the CNTPs by matching the experimental data with conductance simulated using NS-PNP equations for the same CNT geometry (d = 1.5 nm and L = 10 nm) (Figure S1). Unfortunately, we were limited to ion concentrations below 0.25 M because of convergence issues. The fitted surface charge values (Figure 2b) are negative, increase with the concentration, and start to saturate around ion concentration of 0.1 M. As expected, the absolute value of the surface charge at pH 3.0 is lower than at pH 7.5, and, interestingly, the values at pH 3.0 and pH 7.5 are consistently within a factor of 2.2−2.5 within each other. The saturation starts to occur when the surface charge reaches a relatively high value, indicating that this phenomenon could result from cation accumulation inside CNTPs pores blocking additional ions from entering and thus saturating the potential source of the surface charge. Note that our values for the wCNTP surface charge at pH 7.5, which range from −30 to −75 mC/m^2 (which roughly correspond to 10−20 charges over the CNTP surface), are lower than the −40 to −145 mC/m^2 values reported by Bieshuevel and Bazant for larger diameter CNT channels.[23]

Ion Selectivity. We have also studied the ion selectivity of wCNTPs using the reversal potential experiments where we measured the I−V characteristics of the CNTPs in asymmetric ion concentration conditions. We varied the electrolyte concentration in one of the chambers while leaving the concentration in the other chamber constant (See Materials and Methods for details). If a channel has some selectivity to one type of ion, the I−V curve shifts (Figure 3a) and the potential value at which the current becomes zero (*i.e.*, the reversal potential, V_{rev}) can determine the channel permselectivity, P, (see Materials and Methods for details). As we expected from a channel with the negatively charged groups at the entrance, at pH 7.5, wCNTPs showed weak cation

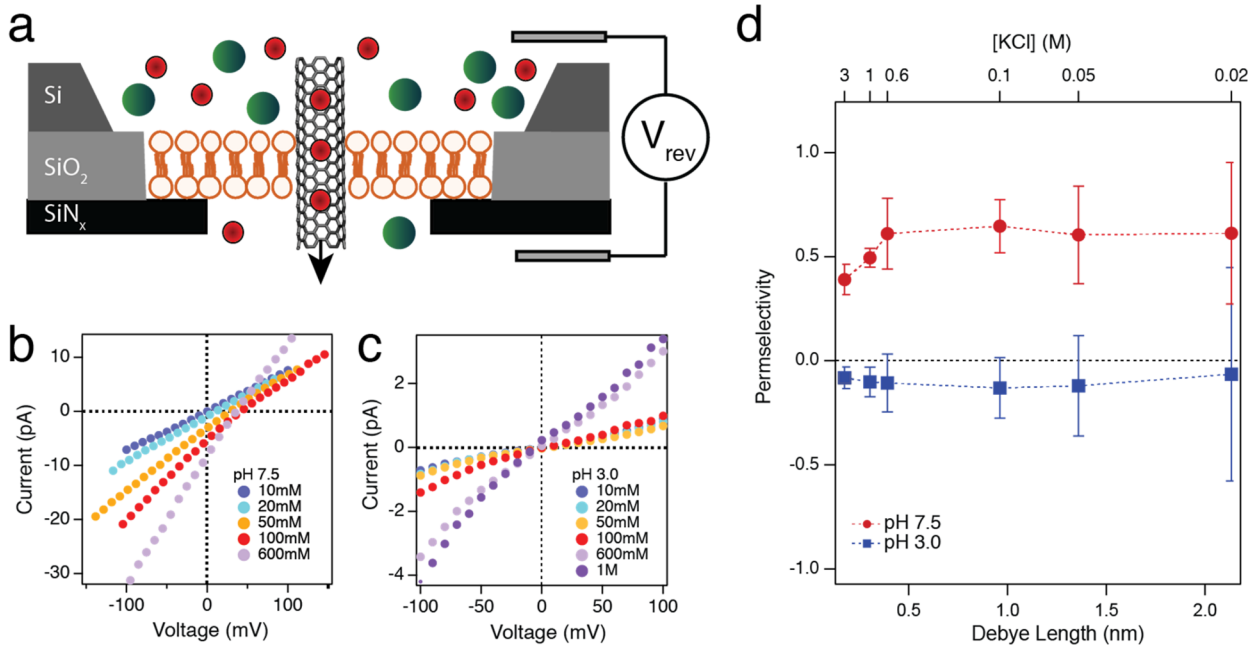

Figure 3. Ion selectivity of 1.5 nm diameter CNTPs. (a) Schematics of the reversal potential measurements showing how preferential transport of one kind of ions across the membrane gives rise to an electric potential. (b, c) I−V curves collected for the reversal potential measurements at pH 7.5 (b) and at pH 3.0 (c). For these experiments, the bottom chamber always contained 10 mM KCl solution, and the concentration of the KCl solution was as indicated on the legend. (d) Permselectivity values measured in these experiments plotted as a function of the Debye length and KCl concentration.

DOI: 10.1021/acsnano.9b05118
ACS Nano 2019, 13, 12851−12859

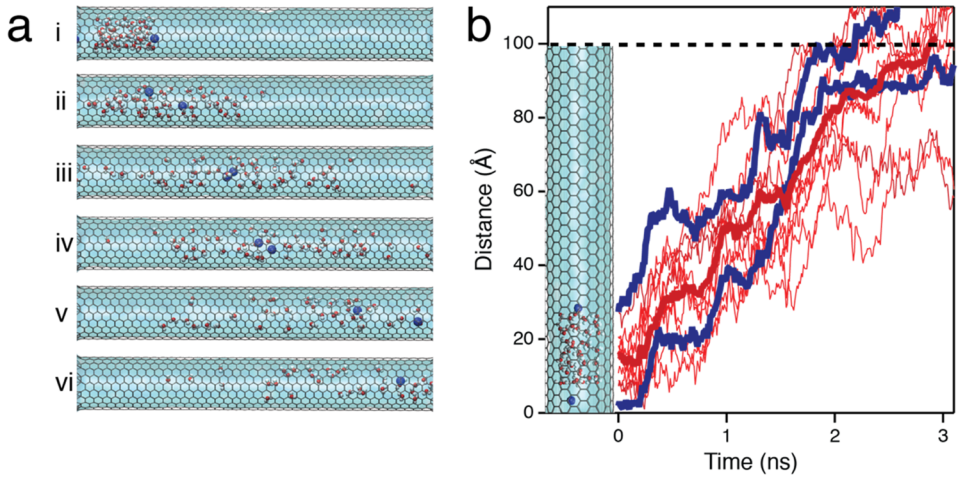

Figure 4. MD simulations of water and ion transport in CNTPs. (a) Snapshots from MD simulations of water and ion transport in 1.5 nm CNTP under an applied electric field showing two K^+ cations (blue) and several water molecules (red) as they move through the CNTP pore (from left to right). The snapshots are numbered sequentially, with the 0.5 ns interval between adjacent frames covering the total duration of 3 ns. (b) Calculated trajectories of K^+ ions (thick blue lines) and water molecules (thin red lines). Thick red line corresponds to the average of 11 water molecule trajectories. The inset image shows the configuration of the system with K^+ ions and water molecules that are being tracked.

selectivity with the permselectivity of *ca.* 0.5, which indicates the cation/anion ratio to be 2−10 depending on the concentration. Unsurprisingly, the channel permselectivity decreased slightly when KCl concentration reached values higher than 600 mM, where the entrance charges became strongly screened (Figure 3d). At pH 3.0, wCNTPs permselectivity dropped down to zero, with the channel showing almost no selectivity between K^+ and Cl^- ions, confirming that the COO− groups at the pore rim were responsible for the channel selectivity at neutral pH values.[9]

We have also investigated the pore selectivity using NS-PNP simulations of the reversal potential experiments using 100 mM as the high concentration and varying the low concentration between 0.1 and 20 mM. The computed permselectivity, which was defined as the ratio of cation and anion currents obtained in the simulations, was 0.585 ± 0.037, which compares favorably with the average value of 0.619 ± 0.019 measured in the experiments at KCl concentrations below 1M.

MD Simulations. To understand the molecular level details of the effect of the surface charge on ion transport in these channels, we have performed non-equilibrium MD simulations of the ion and water flow in CNTPs (see Materials and Methods section for details). The simulations (Figure 4a, see also Supporting Information Movie S1) showed that K^+ cations were rapidly entering and passing through the CNTP channel under an applied electric field of 50 mV/nm. The electroosmotic ion velocities observed in the simulations (Table 1) were quite high owing to the relatively large values of the applied electric field. The cation transport was also accompanied by significant overall flow of water through the channel in the direction of the ion travel. Computed trajectories (Figure 4b) and velocities of water and potassium ions (Table 1) are strongly correlated, indicating that there is a significant overall water flux in the direction of the ion travel, again illustrating the extreme degree of electroosmotic coupling in these channels. Data in Table 1 indicate that water and ion velocities stay constant for low surface charge densities, for example, for $\sigma = -27$ and $\sigma = -54$ mC/m^2. However, as the surface charge density increases to $\sigma = -118$ mC/m^2, the velocities of both water molecules and potassium ions decrease, indicating that for higher surface charge densities, increased adsorption of cations to the CNTP walls can frustrate the slip conditions and cause the flow velocities to decrease.

Table 1. Computed Average Velocity of Water and Potassium Ions in (11,11) CNT with L = 10 nm at a Concentration of 1 M Using MD Simulations

surface charge (mC/m^2)	u_{water} (m/s)	u_{K^+} (m/s)
−27	2.9 ± 0.29	2.31
−54	3.01 ± 0.28	2.45
−114	1.98 ± 0.42	2.15

The calculated electroosmotic ion velocities allow us to estimate the electrophoretic mobility of K^+ ions in 1.5 nm CNTPs. We can interpolate the calculated ion velocities (Table 1) to the surface charge of *ca.* −70 mC/m^2, which would correspond to a relatively high ion concentration regime (Figure 2b). This value (2.37 m/s) at the value of applied field of 50 mV/nm corresponds to the electrophoretic mobility for K^+ ions of 4.9×10^{-8} m^2·V^{-1}·s^{-1}, which is about 40% lower than the bulk value of 7.6×10^{-8} m^2·V^{-1}·s^{-1}. Our value is also very close to the electrophoretic mobility of 5.0×10^{-8} m^2·V^{-1}·s^{-1} reported by Hinds and colleagues for K^+ ion transport in the similar 1.5 nm diameter but significantly thicker (5 μm) SWCNT membranes.[31] Interestingly, in that study Hinds and colleagues did not observe significant electroosmotic flows in unmodified CNTs and had to graft diazonium salts to the nanotube surface to enhance the surface charge, whereas our experiments and simulations indicate that electroosmotic effects remain significant even in unmodified CNT pores.

Strong electroosmotic coupling that is pH-independent, has a high degree of fluid slip at the wCNTP walls leading to low friction flow through the pore, and has very small pore length that produced high electric field values for relatively modest applied voltages all point to the possibility of using unfunctionalized CNTPs as low-voltage electroosmotic

DOI: 10.1021/acsnano.9b05118
ACS Nano 2019, 13, 12851−12859

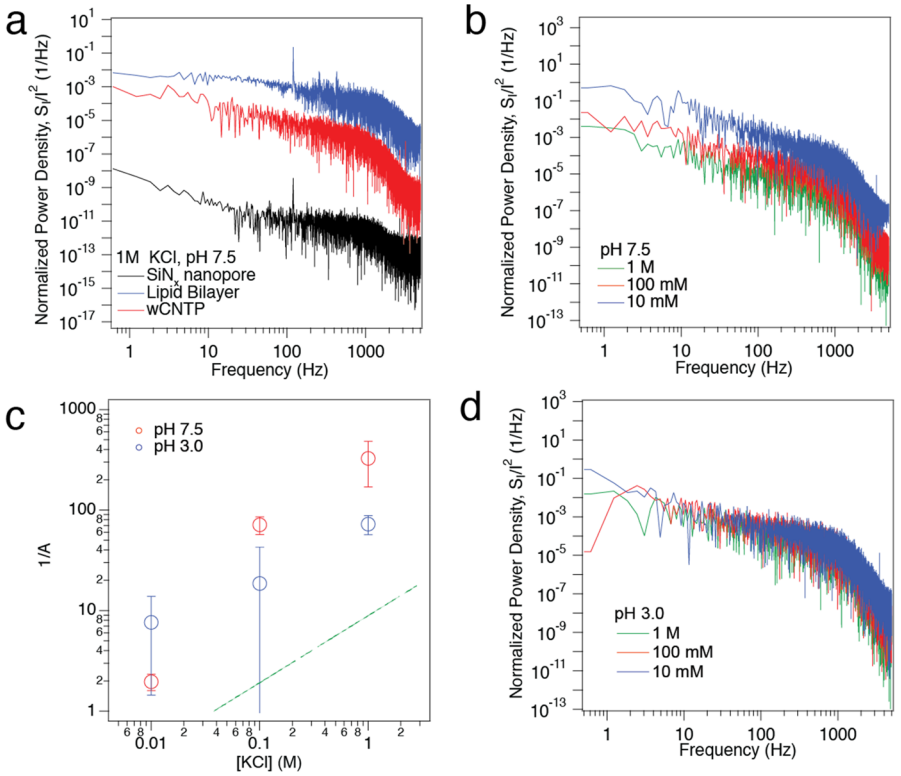

Figure 5. Ionic current noise in wCNTPs. (a) Normalized power spectra of bare SiN_x nanopore, SiN_x nanopore sealed with a lipid bilayer, and wCNTP measured for 1 M KCl electrolyte concentration, +100 mV bias voltage, and pH 7.5. (b, d) Power spectra of wCNTP at pH 7.5 (b) and pH 3.0 (d) measured at different KCl concentrations. (c) Plot of the inverse values of the parameter *A* (see eq 5) fitted to the power spectra as a function of ion concentration. The green dash-dotted line is provided as a guide to the eye and corresponds to the 2/3 power law.

pumps (EOPs). Indeed, our calculated water velocities in CNTPs (Table 1) provide an estimate of the electroosmotic transport figure of merit (FOM) of *ca.* 3.7 $mL{\cdot}cm^{-2}{\cdot}min^{-1}{\cdot}V^{-1}$. This value is at least an order of magnitude higher than the typical FOM values for low-voltage electroosmotic pumps based on porous Si[32] and is the same order of magnitude as the value obtained for EOPs based on chemically functionalized CNT membranes.[31]

Current Noise in CNTPs. Fluctuation of ionic current can provide additional information about the dynamic processes inside the nanotube pores.[33,34] Normalized power spectra of the ion current (Figure 5a) show the expected behavior where the large bare SiN_x pore shows the smallest relative noise, with the CNTP and lipid bilayer showing progressively larger relative noise. The noise spectra represent the combination of white noise, $1/f$ noise, and other noises such as interactions at the channel entrance.[33,35] The noise component that carries the most information about the ion current is the $1/f$ noise, which dominates the low-frequency regime (1−100 Hz), whereas the higher frequencies are dominated by white noise.[33] The $1/f$ noise is observed in electronic current in metals and semiconductors and ionic currents in biological and artificial membrane channels.[36,37] A common approach to analyzing $1/f$ noise is the Hooge's empirical relation, which was first proposed for electronic conductance in homogeneous samples, but later became well-accepted for analyzing ionic current through biological and solid-state nanopore systems.[15,36,38]

$$\frac{S(f)}{I^2} = \frac{A}{f} = \frac{\alpha}{N}\frac{1}{f} \tag{5}$$

where $S(f)$ is power density, f is frequency, I is current, A is noise amplitude, α is a parameter related to temperature and mobility,[34] and N is the number of charge carriers. Hooge's relation states that the normalized power density $S(f)/I^2$ is inversely proportional to the frequency and the proportionality coefficient, A, is itself inversely proportional to the number of charge carriers. Indeed, when we fitted our data to the Hooge's relationship (eq 5) and plotted the values of $1/A$ as a function of ion concentration, we observed that they followed the same 2/3 power law dependence that we saw in ion current measurement (Figure 3c). Interestingly, noise spectra obtained at pH 7.5 show the $1/f$ noise decreasing as the KCl concentration increased (Figure 5b), which likely reflects the increased screening of charges at the pore entrance. Indeed, the noise spectra obtained at different concentrations of KCl at pH 3.0 (Figure 5d) where the CNTP entrance charges are neutralized do not show this trend and instead overlap one another.

CONCLUSIONS

Our results indicate that ion conductance through 1.5 nm diameter CNTs is governed by a complex interplay of phenomena that involve confinement, wall slip, charge equilibria, and above all very strong electroosmotic transport coupling. Significantly, these effects lead to a characteristic $c^{2/3}$ conductance scaling with ion concentration. Continuum NS-PNP simulations and non-equilibrium MD simulations

DOI: 10.1021/acsnano.9b05118
ACS Nano 2019, 13, 12851−12859

revealed the mechanism of this coupling at the molecular scale and provided estimates of electroosmotic transport velocities in this system that indicate that small diameter CNTPs could act as efficient electroosmotic pumping media. Our findings should also help researchers to design the next generations of membranes, separation systems, and microfluidic devices for the applications that require control over water and ion transport on the nanoscale.

MATERIALS AND METHODS

SiN_x Nanopore Chip Fabrication. SiN_x nanopore chips fabrication followed the protocols that we reported previously.[9] Briefly, a 500 μm-thick and 100 mm diameter silicon ⟨100⟩ wafer was cleaned, and 2 μm-thick SiO_2 films were thermally deposited on both sides, followed by 50 nm of SiN_x deposited on both sides of the wafer. 100 nm diameter circular windows were defined by electron-beam lithography on one side of the wafer and etched with SF_6 plasma. Photolithography was used on the other side to define the pattern for KOH etching and buffered oxide etching down to SiN_x membrane. This process produces freestanding SiN_x membranes containing *ca.* 100 nm diameter through-holes. To improve the quality of chips, we additionally utilized atomic layer deposition (ALD) to deposit *ca.* 5−10 nm silicon dioxide (SiO_2) on both sides of chips after plasma cleaning. After the ALD deposition, the chips were cleaned for 20 min in heated Piranha solution: 33% of hydrogen peroxide (35 wt % in H_2O, stabilized, Acros organics, CAS: 7722-84-1) and 66% of sulfuric acid (Merck, GR ACS, CAS: 7664-93-9) for 20 min. After cleaning, the chips were rinsed by and stored in deionized water.

Vesicles Preparation. Preparation of the *ca.* 200 nm diameter large unilamellar vesicles followed a previously described protocol.[9] The lipid composition was 90% 1,2-dioleoyl-*sn*-glycero-3-phosphocholine (DOPC, Avanti, CAS: 4235-95-4) and 10% cholesterol (Sigma, CAS: 57-88-5). Briefly, the mixture of DOPC and cholesterol was dried and then bath sonicated in 200 mM KCl to form lipid vesicles. After 30 min incubation, vesicle solution underwent 10 cycles of freeze and thaw to break possible multilayers. Next, the solution was extruded through a 200 nm filter. The size of final vesicles was verified by dynamic light scattering.

Ion Conductance Measurements. Cleaned SiN_x chips were mounted in a homemade Teflon fluid cell with silicon glue (Ecoflex 5, Smooth-On, Inc.). The cell was equipped with a pair of Ag/AgCl electrodes. For some measurements, 1 M KCl salt bridges (4 wt % agar powder, Alfa Aesar, CAS: 9002−18−0) were used. Conductance characteristics were recorded with a patch clamp amplifier (Axon Instruments, CV 203BU Headstage, Axopatch 200B Integrating Patch Clamp, and Axon CNS Digidata 1440A). The electrolyte solution for the measurements contained potassium chloride (Sigma, CAS: 7447-40-7) TE buffer, 10 mM Trizma base (Sigma, CAS: 77-86-1), and 1 mM EDTA (Sigma-Aldrich, CAS: 60-00-4). Solution pH values were titrated with hydrochloric acid. Conductance values were determined from the slope of the recorded $I-V$ curves. About 20 different wCNTP devices were used and at least three measurements were performed for each concentration and pH value. Conductance measured in this platform matched the values obtained previously in a platform that Montal−Mueller bilayer preparation method.[21] The values obtained from $I-V$ curves also matched the conductance values determined from observing conductance jumps following individual CNTP incorporation events.

Ion Selectivity Determination with Reversal Potential Measurements. To measure ion selectivity, an $I-V$ curve was first recorded using 10 mM KCl in both top and bottom chambers and compensated for any instrumental offsets to the zero-current voltage. The solution of the top chamber was then changed to a different concentration, and an $I-V$ curve was recorded using the fixed original offset. The value of the reversal potential was determined from the new zero-current voltage value and used to derive the ion selectivity using Goldman−Hodgkin−Katz equation:

$$V_{rev} = (2t_+ - 1)\frac{RT}{F}\ln\frac{c_{top}}{c_{bottom}}$$

where V_{rev} is the reversal potential, t_+ is the effective transmembrane number of cation (percentage of cation transferring through membrane out of total ion transfer), c is the electrolyte concentration for either top or bottom chamber, R is the molar gas constant, T is the temperature, and F is the Faraday constant. The permselectivity (P) was then calculated using the cation transport number in bulk (t_{+bulk} = 0.49 for KCl solution) and the following equation:

$$P = \frac{t_+ - t_{+bulk}}{1 - t_{+bulk}}$$

Noise Measurements. The power spectra were determined from the 2 s duration ion current traces collected with the low-pass filter frequency set at 5 kHz.

Continuum Modeling. Ionic transport inside the CNT is described by the coupled Navier−Stokes and Poisson-Nernst−Planck (NS-PNP) equations (see Supporting Information for the detailed model description). The coupled NS-PNP model equations were solved numerically using the OpenFOAM v4.1 (http://www.openfoam.com/) based on the finite volume method.[39,40] Throughout the NS-PNP simulations, we considered a CNT with d = 1.5 nm and L = 10 nm, same as used in the experiment, except for computing the concentration-conductance dependence in Figure 2a where the simulated CNT has a size of d = 14 nm and L = 10 nm. We used an axisymmetric domain (see Figure S1) which allowed us to solve the NS-PNP equations in two dimensions using an unstructured non-uniform mesh with high resolution inside the CNT. The mesh was generated using Gmsh software.[41] We considered two different CNT sizes in our NS-PNP simulations. The first the e only considered the transport of K^+ and Cl^- species, assuming the contribution of H^+ and OH^- is negligible. To check this assumption, we tested the contribution of H^+ and OH^- species on the fitted surface charges for c = 0.01 M and pH = 7.5 and found that the presence of H^+ and OH^- lower the surface charge by only 2 mC/m^2. Water density was set to the bulk density of water (1000 kg/m^3) at room temperature (25 °C), and the relative permittivity was set to 80 in all simulations. Bulk properties of water viscosity (ν = 1.00 × 10^{-6} m^2/s) and the diffusion coefficients of K^+ and Cl^- (D_{K^+} = 1.98 × 10^{-9}m^2/s, and D_{Cl^-} = 2.05 × 10^{-9} m^2/s) at room temperature were used to compute the concentration-conductance of the CNT with d = 14 nm. To improve the continuum prediction at the CNT with d = 1.5 nm, the viscosity of water and the diffusion coefficients of K^+ and Cl^- were calculated using MD simulations and then plugged into the NS-PNP model. The calculated properties are found to be ν = 0.56 × 10^{-6} m^2/s, D_{K^+} = 1.62 × 10^{-9} m^2/s, and D_{Cl^-} = 1.87 × 10^{-9} m^2/s (see Figure S2 for the calculated mean squared displacement (MSD) of both K^+ and Cl^- ions.)

MD Simulations. MD simulations were performed using the LAMMPS package.[42] The CNT structure was generated using VMD,[43] and the initial simulation box was generated using PACKMOL with an ionic concentration of c = 1 M.[44] The system dimensions were selected to be 62 nm × 64 nm × 160 nm in the x, y, and z directions, respectively. We used the extended simple point charge water model and constrained the water molecules using the SHAKE algorithm to maintain the rigidity of each molecule. The Lennard-Jones (LJ) potential parameters are given in Table S1. The cutoff distance for LJ interactions was set to 12 Å. The long-range interactions were computed using the particle-particle-particle-mesh method.[45] For each simulation, we first equilibrated the system for 2 ns at a temperature of 300 K using canonical ensemble (NVT) by Nosè−Hoover thermostat with a time constant of 0.1 ps.[46,47] A time step of 1 fs was used in all simulations. Following equilibration, we applied an electric field to perform non-equilibrium calculations. The simulations were run for 20 ns. For better statistics, we dropped the first 4 ns of the non-equilibrium simulation and considered only the last 16 ns for production.

DOI: 10.1021/acsnano.9b05118
ACS Nano 2019, 13, 12851−12859

ASSOCIATED CONTENT

Supporting Information

The Supporting Information is available free of charge on the ACS Publications website at DOI: 10.1021/acsnano.9b05118.

Additional details of continuum modeling, two figures, and two tables (PDF)

Movie S1 showing water molecules and ions moving through a carbon nanotube, see Figure 4 for additional details and analysis (MP4)

AUTHOR INFORMATION

Corresponding Author

*E-mail: noy1@llnl.gov.

ORCID

Meni Wanunu: 0000-0002-9837-0004

Aleksandr Noy: 0000-0003-4924-2652

Notes

The authors declare no competing financial interest.

ACKNOWLEDGMENTS

We thank Drs. R. Y. Henley and R. H. Tunuguntla for help with the measurement protocols used in this work. CNT synthesis and characterization were supported by the U.S. Department of Energy, Office of Basic Energy Sciences, Division of Materials Sciences and Engineering under award SCW0972. Ion conductance, ion selectivity studies and MD simulations were supported as part of the Center for Enhanced Nanofluidic Transport (CENT), an Energy Frontier Research Center funded by the U.S. Department of Energy, Office of Science, Basic Energy Sciences under award no. DE-SC0019112. Nanopore conductance measurement platform fabrication was supported by the Division of Materials Research of the National Science Foundation under an award 1710211. Work at the Lawrence Livermore National Laboratory was performed under the auspices of the U.S. Department of Energy under contract DE-AC52-07NA27344. Work at the Molecular Foundry was supported by the Office of Science, Office of Basic Energy Sciences, of the U.S. Department of Energy under contract no. DE-AC02-05CH11231. A.T. and N.R.A acknowledge the use of Blue Waters which is provided by the University of Illinois and National Center for Supercomputing Applications supported by NSF awards OCI-0725070 and ACI-1238993 and the State of Illinois.

REFERENCES

(1) Dunn, B.; Kamath, H.; Tarascon, J. M. Electrical Energy Storage for the Grid: A Battery of Choices. *Science* **2011**, *334*, 928−935.

(2) Plett, T.; Thai, M. L.; Cai, J.; Vlassiouk, I.; Penner, R. M.; Siwy, Z. S. Ion Transport in Gel and Gel-Liquid Systems for $LiClO_4$-Doped PMMA at the Meso- and Nanoscales. *Nanoscale* **2017**, *9*, 16232−16243.

(3) Blumwald, E.; Aharon, G. S.; Apse, M. P. Sodium Transport in Plant Cells. *Biochim. Biophys. Acta, Biomembr.* **2000**, *1465*, 140−151.

(4) Hille, B. *Ion Channels of Excitable Membranes*, 3rd ed.; Sinauer: Sunderland, MA, 2001.

(5) Stein, D.; Kruithof, M.; Dekker, C. Surface-Charge-Governed Ion Transport in Nanofluidic Channels. *Phys. Rev. Lett.* **2004**, *93*, 035901.

(6) Bocquet, L.; Charlaix, E. Nanofluidics, from Bulk to Interfaces. *Chem. Soc. Rev.* **2010**, *39*, 1073−1095.

(7) Horner, A.; Pohl, P. Single-File Transport of Water through Membrane Channels. *Faraday Discuss.* **2018**, *209*, 9−33.

(8) Hummer, G.; Rasaiah, J. C.; Noworyta, J. P. Water Conduction through the Hydrophobic Channel of a Carbon Nanotube. *Nature* **2001**, *414*, 188−190.

(9) Tunuguntla, R.; Henley, R.; Yao, Y.-C.; Pham, T. A.; Wanunu, M.; Noy, A. Enhanced Water Permeability and Tunable Ion Selectivity in Sub-Nanometer Carbon Nanotube Porins. *Science* **2017**, *357*, 792−796.

(10) Holt, J. K.; Park, H. G.; Wang, Y.; Stadermann, M.; Artyukhin, A. B.; Grigoropoulos, C. P.; Noy, A.; Bakajin, O. Fast Mass Transport Through Sub-2-Nanometer Carbon Nanotubes. *Science* **2006**, *312*, 1034−1037.

(11) Secchi, E.; Marbach, S.; Niguès, A.; Stein, D.; Siria, A.; Bocquet, L. Massive Radius-Dependent Flow Slippage in Carbon Nanotubes. *Nature* **2016**, *537*, 210−213.

(12) Siria, A.; Poncharal, P.; Biance, A. L.; Fulcrand, R.; Blase, X.; Purcell, S. T.; Bocquet, L. Giant Osmotic Energy Conversion Measured in a Single Transmembrane Boron Nitride Nanotube. *Nature* **2013**, *494*, 455−458.

(13) Esfandiar, A.; Radha, B.; Wang, F. C.; Yang, Q.; Hu, S.; Garaj, S.; Nair, R. R.; Geim, A. K.; Gopinadhan, K. Size Effect in Ion Tansport through Angstrom-Scale Silts. *Science* **2017**, *358*, 511−513.

(14) Fumagalli, L.; Esfandiar, A.; Fabregas, R.; Hu, S.; Ares, P.; Janardanan, A.; Yang, Q.; Radha, B.; Taniguchi, T.; Watanabe, K.; Gomila, G.; Novoselov, K. S.; Geim, A. K. Anomalously Low Dielectric Constant of Confined Water. *Science* **2018**, *360*, 1339−1342.

(15) Secchi, E.; Niguès, A.; Jubin, L.; Siria, A.; Bocquet, L. Scaling Behavior for Ionic Transport and Its Fluctuations in Individual Carbon Nanotubes. *Phys. Rev. Lett.* **2016**, *116*, 154501.

(16) Smeets, R. M.; Keyser, U. F.; Krapf, D.; Wu, M.-Y.; Dekker, N. H.; Dekker, C. Salt Dependence of Ion Transport and DNA Translocation through Solid-State Nanopores. *Nano Lett.* **2006**, *6*, 89−95.

(17) Amiri, H.; Shepard, K. L.; Nuckolls, C.; Hernández Sánchez, R. Single-Walled Carbon Nanotubes: Mimics of Biological Ion Channels. *Nano Lett.* **2017**, *17*, 1204−1211.

(18) Corry, B. Water and Ion Transport through Functionalized Carbon Nanotubes: Implications for Desalination Technology. *Energy Environ. Sci.* **2011**, *4*, 751−759.

(19) Majumder, M.; Chopra, N.; Andrews, R.; Hinds, B. J. Nanoscale Hydrodynamics: Enhanced Flow in Carbon Nanotubes. *Nature* **2005**, *438*, 44−45.

(20) Wu, J.; Gerstandt, K.; Zhang, H.; Liu, J.; Hinds, B. J. Electrophoretically Induced Aqueous Flow through Single-Walled Carbon Nanotube Membranes. *Nat. Nanotechnol.* **2012**, *7*, 133−139.

(21) Geng, J.; Kim, K.; Zhang, J.; Escalada, A.; Tunuguntla, R.; Comolli, L. R.; Allen, F. I.; Shnyrova, A. V.; Cho, K. R.; Munoz, D.; Wang, Y. M.; Grigoropoulos, C. P.; Ajo-Franklin, C. M.; Frolov, V. A.; Noy, A. Stochastic Transport through Carbon Nanotubes in Lipid Bilayers and Live Cell Membranes. *Nature* **2014**, *514*, 612−615.

(22) Tunuguntla, R. H.; Escalada, A.; Frolov, V. A.; Noy, A. Synthesis, Lipid Membrane Incorporation, and Ion Permeability Testing of Carbon Nanotube Porins. *Nat. Protoc.* **2016**, *11*, 2029−2047.

(23) Biesheuvel, P. M.; Bazant, M. Z. Analysis of Ionic Conductance of Carbon Nanotubes. *Phys. Rev. E* **2016**, *94*, 050601.

(24) Feng, J.; Liu, K.; Graf, M.; Dumcenco, D.; Kis, A.; Di Ventra, M.; Radenovic, A. Observation of Ionic Coulomb Blockade in Nanopores. *Nat. Mater.* **2016**, *15*, 850−855.

(25) Kowalczyk, S. W.; Grosberg, A. Y.; Rabin, Y.; Dekker, C. Modeling the Conductance and DNA Blockade of Solid-State Nanopores. *Nanotechnology* **2011**, *22*, 315101.

(26) Lee, C. Y.; Choi, W.; Han, J. H.; Strano, M. S. Coherence Resonance in a Single-Walled Carbon Nanotube Ion Channel. *Science* **2010**, *329*, 1320−1324.

(27) Grosjean, B.; Pean, C.; Siria, A.; Bocquet, L.; Vuilleumier, R.; Bocquet, M.-L. Chemisorption of Hydroxide on 2D Materials from DFT Calculations: Graphene versus Hexagonal Boron Nitride. *J. Phys. Chem. Lett.* **2016**, *7*, 4695−4700.

DOI: 10.1021/acsnano.9b05118
ACS Nano 2019, 13, 12851−12859

(28) Uematsu, Y.; Netz, R. R.; Bocquet, L. r.; Bonthuis, D. J. Crossover of the Power-Law Exponent for Carbon Nanotube Conductivity as a Function of Salinity. *J. Phys. Chem. B* **2018**, *122*, 2992−2997.
(29) Lokesh, M.; Youn, S. K.; Park, H. G. Osmotic Transport across Surface Functionalized Carbon Nanotube Membrane. *Nano Lett.* **2018**, *18*, 6679−6685.
(30) Manghi, M.; Palmeri, J.; Yazda, K.; Henn, F.; Jourdain, V. Role of Charge Regulation and Flow Slip in the Ionic Conductance of Nanopores: An Analytical Approach. *Phys. Rev. E* **2018**, *98*, 012605.
(31) Wu, J.; Gerstandt, K.; Majumder, M.; Zhan, X.; Hinds, B. J. Highly Efficient Electroosmotic Flow through Functionalized Carbon Nanotube Membranes. *Nanoscale* **2011**, *3*, 3321−3328.
(32) Yao, S.; Myers, A. M.; Posner, J. D.; Rose, K. A.; Santiago, J. G. Electroosmotic Pumps Fabricated from Porous Silicon Membranes. *J. Microelectromech. Syst.* **2006**, *15*, 717−728.
(33) Neumcke, B. 1/f Noise in Membranes. *Biophys. Struct. Mech.* **1978**, *4*, 179−199.
(34) Verveen, A. A.; DeFelice, L. J. Membrane Noise. *Prog. Biophys. Mol. Biol.* **1974**, *28*, 189−265.
(35) Antonov, V. F. *Lipids and Ionic Permeability of Membranes*; Nauka: Moscow, 1982; p 150.
(36) Bezrukov, S. M.; Irkhin, A. I.; Sibilev, A. I. An Upper Estimate for 1/F Noise Intensity in Ionic Conductors from Experiments with a Molecular Microcontact. *Phys. Lett. A* **1987**, *123*, 477−480.
(37) Hooge, F. N.; Hoppenbrouwers, A. M. 1/f-Noise in Continuous Thin Gold Films. *Physica* **1969**, *45*, 386−392.
(38) Smeets, R. M.; Keyser, U. F.; Dekker, N. H.; Dekker, C. Noise in Solid-State Nanopores. *Proc. Natl. Acad. Sci. U. S. A.* **2008**, *105*, 417−421.
(39) Nandigana, V. V.; Aluru, N. R. Understanding Anomalous Current-Voltage Characteristics in Microchannel-Nanochannel Interconnect Devices. *J. Colloid Interface Sci.* **2012**, *384*, 162−171.
(40) Feng, J.; Graf, M.; Liu, K.; Ovchinnikov, D.; Dumcenco, D.; Heiranian, M.; Nandigana, V.; Aluru, N. R.; Kis, A.; Radenovic, A. Single-Layer MoS_2 Nanopores as Nanopower Generators. *Nature* **2016**, *536*, 197−200.
(41) Geuzaine, C.; Remacle, J.-F. Gmsh: A 3-D Finite Element Mesh Generator with Built-In Pre- and Post-Processing Facilities. *Int. J. Numer. Methods Eng.* **2009**, *79*, 1309−1331.
(42) Plimpton, S. Fast Parallel Algorithms for Short-Range Molecular Dynamics. *J. Comput. Phys.* **1995**, *117*, 1−19.
(43) Humphrey, W.; Dalke, A.; Schulten, K. VMD: Visual Molecular Dynamics. *J. Mol. Graphics* **1996**, *14*, 33−38.
(44) Martinez, L.; Andrade, R.; Birgin, E. G.; Martinez, J. M. PACKMOL: A Package for Building Initial Configurations for Molecular Dynamics Simulations. *J. Comput. Chem.* **2009**, *30*, 2157−2164.
(45) Hockney, R. W.; Eastwood, J. W. *Computer Simulation Using Particles*; Taylor & Francis, Inc.: New York, 1988; p 564.
(46) Nosé, S. A Unified Formulation of the Constant Temperature Molecular Dynamics Methods. *J. Chem. Phys.* **1984**, *81*, 511−519.
(47) Hoover, W. G. Canonical Dynamics: Equilibrium Phase-Space Distributions. *Phys. Rev. A: At., Mol., Opt. Phys.* **1985**, *31*, 1695−1697.

DOI: 10.1021/acsnano.9b05118
ACS Nano 2019, 13, 12851−12859